



Quantifying the historic and future response of karst spring discharge to climate variability and change at a snow-influenced temperate catchment in central Europe

Xinyang Fan^{1,2} · Nadine Goeppert¹ · Nico Goldscheider¹

Received: 10 January 2023 / Accepted: 18 August 2023
© The Author(s) 2023

Abstract

Climate change is projected to threaten groundwater resources in many regions, but projections are highly uncertain. Quantifying the historic impact potentially allows for understanding of hydrologic changes and increases confidence in the predictions. In this study, the responses of karst discharge to historic and future climatic changes are quantified at Blautopf Spring in southern Germany, which is one of the largest karst springs in central Europe and belongs to a regional aquifer system relevant to the freshwater supply of millions of people. Statistical approaches are first adopted to quantify the hydrodynamic characteristics of the karst system and to analyse the historic time series (1952–2021) of climate variables and discharge. A reservoir model is then calibrated and evaluated with the observed discharge and used to simulate changes with three future climate-change scenarios. Results show that changes in the annual mean and annual low discharge were not significant, but the annual peak discharge shifted to a low state ($<13.6 \text{ m}^3 \text{ s}^{-1}$) from 1988 onwards due to decreasing precipitation, increasing air temperature, and less intense peak snowmelt. The peak discharge may decrease by 50% in this century according to the projections of all climate-change scenarios. Despite there being no significant historic changes, the base flow is projected to decrease by 35–55% by 2100 due to increasing evapotranspiration. These findings show the prolonged impact of climate change and variability on the floods and droughts at the springs in central Europe, and may imply water scarcity risks at similar climatic and geologic settings worldwide.

Keywords Karst · Spring discharge · Climate change · Conceptual modelling · Germany

Introduction

Climate change is projected to impact groundwater resources globally (IPCC 2014, 2021); many countries and regions may face declining groundwater levels such as the US, India, and Germany (Amanambu et al. 2020; Wunsch et al. 2022). Compared with porous aquifers, karst aquifers are potentially more sensitive to climate change, as their fast flow paths respond quickly to reduced recharge due to decreasing precipitation and increasing temperature (Hartmann et al.

2017). Being a vital freshwater resource, karst aquifers and springs play a vital role in fulfilling the drinking water needs of ~9.2% of the global population (Stevanović 2019). Understanding their changes is thus crucial for sustainably managing the usage while meeting the increasing demands of climate change and population growth (Mahler et al. 2021).

Many studies have attempted to project groundwater changes in the future climate by using groundwater models (e.g. MODFLOW, MIKE SHE) which take future meteorological variables either derived from global climate models (GCMs) and regional climate models (RCMs; Toews and Allen 2009; Kumar 2012; Doummar et al. 2018; Amanambu et al. 2020) or by applying a change factor to the historic climate (Chen et al. 2018; Dubois et al. 2020). However, the exact magnitudes of model projections are often highly uncertain due to (1) the influential drivers of groundwater, which are considered static in the model but are subjected to change, such as agricultural irrigation, land use and land cover changes, natural climate variations, and anthropogenic

✉ Xinyang Fan
xinyang.fan@partner.kit.edu

¹ Institute of Applied Geosciences, Division of Hydrogeology, Karlsruhe Institute of Technology (KIT), 76131 Karlsruhe, Germany

² Department of Infrastructure Engineering & Melbourne Climate Futures Academy, University of Melbourne, Melbourne 3053, Australia

climate change (Green et al. 2011; Hartmann et al. 2014; Goderniaux et al. 2015); (2) the delayed response of groundwater to climate change (Panagopoulos and Lambrakis 2006; Hosseini et al. 2017); (3) the highly variable precipitation under climate change, and the increasing temperature that impacts not only evapotranspiration but also the timing of snowmelt (Chen et al. 2018; Lorenzi et al. 2022).

Quantifying the historic impact of climate change on groundwater contributes to understanding the causes of the change and increases confidence in the model projections. Analysing long-term hydrographs at natural catchments potentially allows for the assessment of this impact (Peterson and Western 2014; Ravbar et al. 2018). However, very few studies have quantified the historic impact due to the heterogeneous subsurface properties and flow processes (e.g. exchange between groundwater and surface water; Hartmann et al. 2014; Bonotto et al. 2022), multiple influential drivers of groundwater (e.g. pumping, land use changes, human activities; Shapoori et al. 2015; Kovačič et al. 2020), and lack of long-term groundwater observations (Taylor et al. 2013; Olarinoye et al. 2020). These issues are particularly outstanding for karst aquifers. Due to limited lengths of records and complicated hydrogeological characteristics, a few studies have investigated the water availability in the karst regions within a time frame of 20 years (Xanke and Liesch 2022; Lorenzi et al. 2022). Only a handful of studies have assessed the trends over a half-century (Kimmeier and Bouzelboudjen 2001; Fiorillo et al. 2015, 2021; Leone et al. 2021), and some of them struggled to attribute the trend of changes to climate change (Bonacci 2007). The long-term historic impact of climate change and variations on karst aquifers and springs is thus still largely unknown.

Climate change impacts the global water cycle and its impact is spatially variable because of the varying precipitation patterns and changing land surface-atmosphere feedbacks (IPCC 2021). Downscaling the global impact to the local scale potentially allows water managers and policymakers to understand the impact on their managing sites and regulate groundwater usage and licence the pumping limits accordingly. Besides that, new methodologies can be best developed at the local scale through analysis in great detail, then generalised and transferred to other sites. Complementing research at the global scale with detailed research at the local scale is thus necessary.

This study aims to establish and test an integrated approach to quantify the impact of climate variability and change on karst spring discharge from both historic and future perspectives. The proposed workflow of this approach is to (1) quantify the hydrodynamic characteristics of the karst system and the historic trends of the climate variables and discharge by using statistical approaches; (2) build up a lumped parameter model for the karst site and evaluate it with the knowledge learned from the historic analysis; and

(3) use the model to simulate future discharge changes under climate change. Step 1 is widely lacking in the studies which attempted to project future water resource changes (Toews and Allen 2009; Kumar 2012; Amanambu et al. 2020), but it is crucial for understanding the hydrological behaviour of the system and the projected future changes. The Blautopf spring in southern Germany is studied, as it is one of the largest and most important karst springs in central Europe (Ufrecht et al. 2016). It drains a large catchment and belongs to Germany's largest karst aquifer system (Swabian-Franconian Alb), which is essential to the drinking water supply of millions of people (Fahrmeier et al. 2022). Quantifying the response of the Blautopf system contributes to understanding the changes of karst aquifers and springs in the temperate climates where around 19% of the land surface consists of carbonate rocks (Goldscheider et al. 2020). The research questions below are answered in this article:

1. What are the historic climatic changes at the study site, in terms of temperature, evapotranspiration, precipitation, intensity and duration of snowmelt?
2. Did the observed climatic changes impact the karst discharge? If yes, what was the impact on the mean, low, and high flow, as well as the intensity and duration of hydrological extremes?
3. Assuming the IPCC climate change scenarios, how will the climate and discharge (minimum, mean, maximum) change at this type of climatic and hydrogeological setting (temperate, snow-influenced karst system) by the end of the twenty-first century?

Study site

The Blautopf spring is located at the southern margin of the Swabian-Franconian Jura Mountains, Germany's largest karst landscape and karst aquifer system. The spring catchment covers an area of ~165 km² delineated by numerous tracer tests and diving explorations (Armbruster et al. 2006; Ufrecht et al. 2016). The catchment drips gradually from northwest to southeast in a range of 878 to 609 m asl. (Fig. 1). The land surface is mainly covered by forests (~31%) and agriculture (~60%) (Köberle 2005; Lauber et al. 2014). Numerous dolines and dry valleys are visible on the land surface. Underneath the landscape is a spectacular and large cave system. The catchment is divided into two subzones by two major caves: the Blue Cave ("Blauhöhle" in German, ~14.6 km length) and the Hessenhau Cave ("Hessenhauhöhle" in German, ~6.0 km length; Schwarz et al. 2009). Each subcatchment is estimated to contribute approximately half of the spring discharge, which is the only known direct outlet of this catchment (Lauber et al. 2013, 2014). The vertical profile shows that

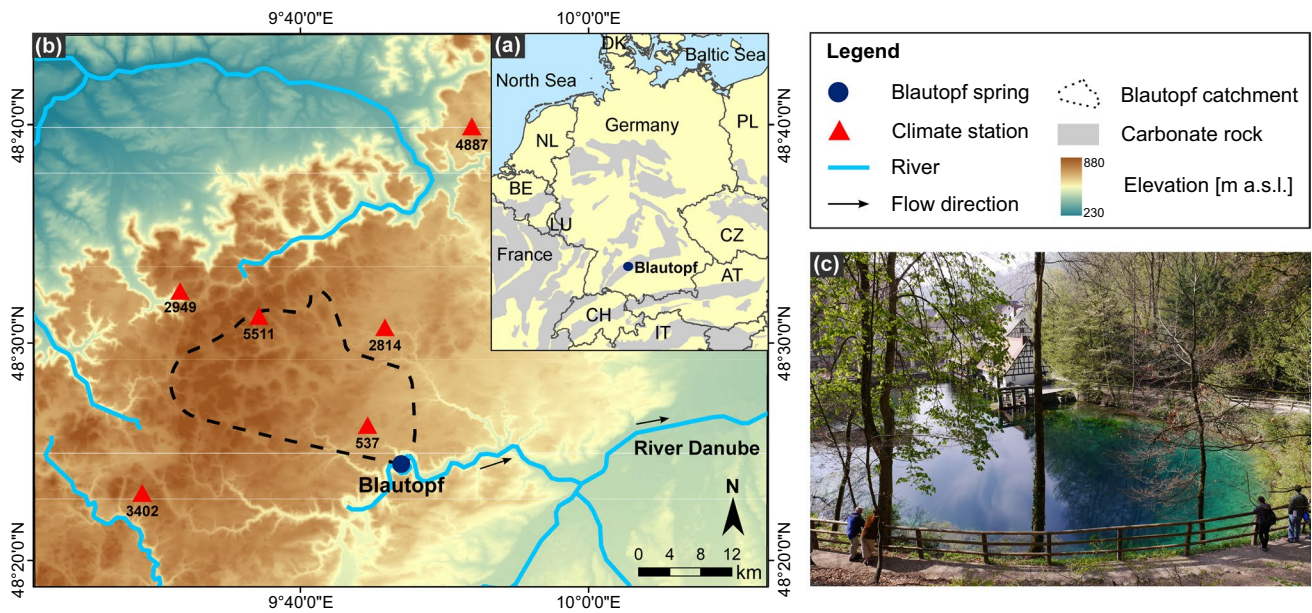


Fig. 1 Location and map of the Blautopf spring and catchment. **a** Distribution of carbonate rocks in Germany and nearby countries (Chen et al. 2017), with the location of Blautopf indicated. **b** Map of

the Blautopf catchment and spring and its nearby climate stations and river networks. **c** A view from the top of the Blautopf spring (photo: N. Goldscheider)

the catchment consists of multiple layers of Upper Jurassic limestone and marl (Selg and Schwarz 2009). The thick saturated (50–120 m) and unsaturated zones (100–150 m) allow a considerable storage capacity of the karst system (Schwarz et al. 2009).

Data and methods

Karst discharge data

The karst spring discharge (Q) recorded at station (ID 76273) from 1 Jan 1952 to 31 Dec 2021 was used in this study and obtained from the Baden-Württemberg State Office for Environment (LUBW). Records show that the discharge was estimated with the stage–discharge relationship from 1952 to 2004. Since 2005, the discharge was calculated as the discharge difference between the downstream and upstream rivers. The discharge calculated with

both methods provides consistent results [Section S1 in the electronic supplementary material (ESM)]. The data were recorded in the hourly interval from 1952 to 2016 and the 15-min interval from 2016 onwards. After removing errors, the data show no daily gap. The subdaily data were then used to calculate the daily, monthly, seasonal, and annual mean discharge.

Climate data

The daily precipitation (P), mean air temperature (T), snow height (SH), and snow water equivalent (SWE) data of the nearby weather stations (Fig. 1) were used to estimate the catchment climate. The data were obtained from the Climate Data Center of Germany (Deutscher Wetterdienst 2021). Table 1 summarises the observed climate variables and the locations of the stations.

The observed precipitation at each station has a data missing rate of <1.5%. The temporal data gaps of each station

Table 1 The weather stations near the Blautopf catchment (locations shown in Fig. 1). Note, the elevation of Station 3402 was 721 m asl (48.4065° N, 9.4928° E) before 1989

Station ID	Longitude [° E]	Latitude [° N]	Elevation [m asl]	Data length	Climate variables
2814	9.7644	48.5122	687	1952–2021	P
5511	9.6187	48.5206	825	1952–2021	P
537	9.7443	48.4369	705	1952–2021	P
3402	9.4837	48.3851	755	1952–2021	P, T, SH, SWE
4887	9.8648	48.6656	734	1952–2016	T, SH, SWE
2949	9.5275	48.5396	758	1952–2001	T, SH, SWE

were filled with the mean precipitation of the other stations on that day. The catchment precipitation was estimated with the Thiessen polygon method in which each station takes a weight of 50.3% (ID 5511), 37.6% (ID 537), 8.4% (ID 2814), and 3.7% (ID 3402). The observed daily mean air temperature at station 3402 with no temporal gap was used to represent the catchment temperature.

The Blautopf catchment was influenced by snow between October and April. Both SH and SWE data were recorded as accumulations of previous and new snow. The daily SH data had only one missing datum which was filled with the mean snow heights of the neighbouring days. Because of snow compaction, the SH data were only used to indicate the days when the catchment was covered by snow; the SWE data were used to represent the snow amount and were nearly in the weekly interval. To interpolate it to daily, the SWE data were first filled with 0 on the days when the SH was 0 and the remaining gaps were then filled by linear interpolation (note that small snow events, which resulted in 2–3 days of snow cover, between two zeros in the weekly SWE time series were not accounted). The degree-day factor (DDF) method (Martinec 1960; Çallı et al. 2022) was adopted to represent the snowmelt processes:

$$\text{Snow}_i = \begin{cases} \text{Snow}_{i-1} + P_i, T_i \leq T_M \\ \max(\text{Snow}_{i-1} - \text{Melt}_i, 0), T_i > T_M \end{cases} \quad (1)$$

$$\text{Lw}_i = \begin{cases} 0, T_i \leq T_M \\ P_i + \min(\text{Snow}_{i-1}, \text{Melt}_i), T_i > T_M \end{cases} \quad (2)$$

$$\text{Melt}_i = \begin{cases} 0, T_i \leq T_M \\ \text{DDF} \times (T_i - T_M), T_i > T_M \end{cases} \quad (3)$$

where P_i is the daily precipitation [mm] for day i , T_i is the daily mean temperature [°C], T_M is the temperature threshold above which the snowmelt occurs, Snow_i is the snow storage [mm day⁻¹], Melt_i is the snowmelt amount [mm day⁻¹], Lw_i is the liquid water [mm day⁻¹] that is available to infiltrate into the subsurface, and DDF is the degree-day factor (DDF) [mm °C⁻¹ day⁻¹]. The DDF (0.1–10) and T_M (–1, 0, 1 °C) are the calibration parameters, and the best set of these was determined to be the one that gives the best estimates of snow storage compared with the observed SWE (Fig. S2 in the ESM).

The daily potential evapotranspiration (PET) of the catchment was estimated with a temperature-based method (Oudin et al. 2005):

$$\text{PET} = \frac{R_e}{\lambda \rho} \frac{T_a + 5}{100}, \text{ if } T_a + 5 > 0 \quad (4)$$

$$\text{PET} = 0, \text{ otherwise} \quad (5)$$

where PET is given in the unit of millimetre per day [mm day⁻¹], R_e is the extra-terrestrial radiation [MJ m⁻² day⁻¹] estimated with the FAO method by using catchment latitude and Julian day (Allen et al. 1998 and Section S2.2 in the ESM), λ is the latent heat flux (=2.45 MJ kg⁻¹), ρ is the water density [kg m⁻³], and T_a is the daily mean air temperature [°C].

Statistical analysis

The hydrodynamic characteristics of the karst system were analysed by using the correlations between the daily precipitation and discharge from 1952 to 2021. The autocorrelation and cross-correlation were calculated with the *acf* and *ccf* functions in the R *stats* package. The autocorrelation of discharge informs (1) the karstification degree of the system and the existence of fast and slow flow paths indicated by the slope of the function (Padilla and Pulido-Bosch 1995; Panagopoulos and Lambrakis 2006), and (2) the karst system memory which refers to the time that the water needs to flow through the karst aquifer and is determined as the time lag at which the function coefficient decreases to 0.2 (Mangin 1984; Benavente et al. 1985; Larocque et al. 1998). The cross-correlation function quantifies the response time of the discharge to precipitation at the time lag when the maximum coefficient is achieved (Panagopoulos and Lambrakis 2006).

The long-term trends of discharge and climate variables were quantified from monthly to annual scales by using the nonparametric Mann–Kendall test (Mann 1945; Kendall 1955) and Sen's slope method (Sen 1968). A MATLAB function *mannkendall v1.0.0* (Collaud Coen et al. 2020; Collaud Coen and Vogt 2021) was used to first remove the first-order autocorrelation in the data with a 3PW prewhitening procedure and then to quantify the trends. To identify any abrupt changes in the data, a Bayesian change-point detection and time-series decomposition algorithm called *Rbeast* (Zhao et al. 2019b) was applied. This algorithm uses a Bayesian model averaging scheme and the Markov Chain Monte Carlo stochastic sampling approach to approximate the complex relationships in the data (Zhao et al. 2019a). The results include the locations of the change points and their probability. In this study, the period was set to 1 in the algorithm for the annual time-series data.

Karst discharge modelling

Historical simulation

A reservoir model, *KarstMod* (Mazzilli et al. 2019), was used to simulate the time-series discharge under historic climate variations. This model was set up with three compartments (E, M, C; Fig. 2), whereby E represents the infiltration zone (soil and epikarst) which is recharged

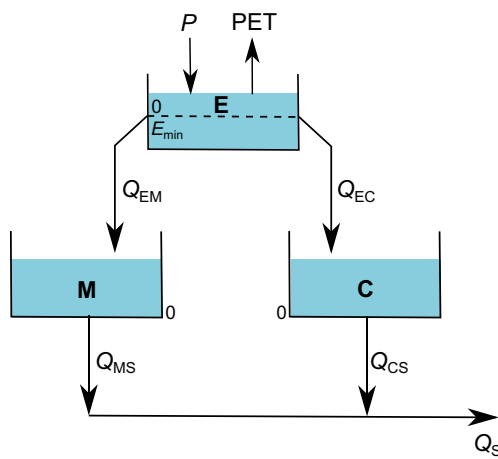


Fig. 2 The model structure adopted to simulate the storage and flow dynamics of the Blautopf system

by precipitation and loses water into the atmosphere via evapotranspiration, and M and C represent the fissured rock matrix and conduits in the underground subsystems. The equations of the model are provided in the following (Mazzilli et al. 2019):

$$\frac{dE}{dt} = P - PET - Q_{EM} - Q_{EC}, \text{ if } E \geq 0 \quad (6)$$

$$\frac{dE}{dt} = P - PET, \text{ if } E_{\min} < E < 0 \quad (7)$$

$$\frac{dM}{dt} = Q_{EM} - Q_{MS} \quad (8)$$

$$\frac{dC}{dt} = Q_{EC} - Q_{CS} \quad (9)$$

$$Q_{EM} = k_{EM} \times E_t, \text{ if } E_t > 0, \text{ otherwise } Q_{EM} = 0 \quad (10)$$

$$Q_{EC} = k_{EC} \times E_t, \text{ if } E_t > 0, \text{ otherwise } Q_{EC} = 0 \quad (11)$$

$$Q_{MS} = k_{MS} \times M_t, \text{ if } M_t > 0, \text{ otherwise } Q_{MS} = 0 \quad (12)$$

$$Q_{CS} = k_{CS} \times C_t, \text{ if } C_t > 0, \text{ otherwise } Q_{CS} = 0 \quad (13)$$

$$Q_S = R_A \times (Q_{MS} + Q_{CS}) \quad (14)$$

where E_t , M_t , and C_t represent the water levels [mm] in the compartments E, M, and C at the time t ; E_{\min} [mm] represents the water holding capacity (of the soil and epikarst) over which the water flows from E into M and C; Q_{AB} represents the flow [mm day⁻¹] from compartment A to B (e.g. E to M), and k_{AB} represents the recession coefficient of the

flow; Q_S represents the spring discharge [m³ s⁻¹]; R_A represents the recharge area [km²].

The model took the daily transformed precipitation (with the DDF method) and PET as inputs to simulate the daily discharge from 1952 to 2021. Three phases were defined in the model: warm-up (1952–1956), calibration (1957–2007) and validation (2008–2021). The model was calibrated by using a quasi-Monte-Carlo approach with a Sobol sequence sampling of the parameter space (Sobol 1976; Mazzilli et al. 2019). Five parameters (k_{EM} , k_{EC} , k_{MS} , k_{CS} , and R_A) were calibrated and 10,000 parameter sets were generated (parameter descriptions and values provided in Table S5 in the ESM). The parameter sensitivity was calculated with the Sobol index (Saltelli 2002) and the model performance was evaluated with the Nash-Sutcliffe efficiency (NSE) coefficient (Nash and Sutcliffe 1970):

$$NSE = 1 - \frac{\sum (Q_{\text{obs}} - Q_{\text{sim}})^2}{\sum (Q_{\text{obs}} - Q_{\text{mean}})^2} \quad (15)$$

where Q_{obs} is the daily observed spring discharge [m³ s⁻¹], Q_{sim} is the daily simulated discharge [m³ s⁻¹], and Q_{mean} is the average of the observed discharge [m³ s⁻¹]. An NSE = 1 represents the best model performance and 0 means the model performance equivalent to using the observed mean discharge.

Simulation of future climate change impacts

The discharge was simulated with the calibrated model from 2006 to 2100 under three climate change scenarios in the 5th Phase of the Coupled Model Intercomparison Project (CMIP5): representative concentration pathways (RCPs) 2.6, 4.5, and 8.5 (most extreme scenario). Each RCP has an ensemble of climate projections generated with the GCMs which are coupled with the RCMs for estimating regional climate change. The GCM-RCM members that represent >80% of the climate spread of all model projections were adopted in this study (Deutscher Wetterdienst 2018). This criterion resulted in five GCM-RCM members being selected for RCP 2.6 and six members for RCPs 4.5 and 8.5 respectively (Table S2 in the ESM). The climate data of the adopted members were bias-corrected and downscaled to 5 km × 5 km by Brienens et al. (2020).

The daily precipitation and air temperature were extracted from each GCM-RCM member at the locations of the observed weather stations (ID 5511, 2814, 3402, 537 in Table 1). The climate data at each location was calculated as the mean of the surrounding 3 × 3 cells of the gridded climate outputs (Wunsch et al. 2022). The future catchment climates were estimated with the same methods as in section “Climate data”—that is, the catchment precipitation and temperature

were estimated by spatially interpolating the extracted climate data using the Thiessen polygon method; the precipitation was transformed into the time-series liquid water with the DDF method; the PET was estimated with the method of Oudin et al. (2005). The daily transformed precipitation and PET of each GCM-RCM member were then taken by the model to simulate the discharge for each climate change scenario. The trends of the simulated annual minimum (2.5th percentile), maximum (97.5th percentile), and mean discharge and climates were quantified with the nonparametric Mann–Kendall test and Sen’s slope method (Mann 1945; Kendall 1955; Sen 1968) as in section “Statistical analysis”.

Results

Karst system hydrodynamics

The cross-correlation function of the daily precipitation and discharge (Fig. 3a) shows that the discharge responds to precipitation with a lag of 3 days. The quick response of the discharge to precipitation confirms the existence of fast flow paths in the karst system. The small peak coefficient (0.22) indicates that the precipitation signal has been strongly attenuated before flowing out to the spring. Following the maximum, no other peak is observed, indicating that one primary quick flow component exists in the system.

The autocorrelation function of the daily precipitation decreases rapidly to 0 (Fig. 3b), indicating no autocorrelation in the data and that precipitation can be treated as a random variable. In contrast, the daily discharge shows strong autocorrelation and the system is estimated to have a memory of 40 days at the coefficient of 0.2. The changing gradients of the function between the time lags indicate the existence of both fast and slow flow components in the system. The coefficient decreases quickly from 1 to 0.5 in the first 11 days because of the fast flow and then reduces slowly,

such as between the intervals of 11–16 days and 17–43 days because of the slow flow components. Overall, this karst system has highly karstified flow paths which allow the system to respond quickly to rainfall and snowmelt, and it also has a large storage capacity and fissured karst matrix as reflected by the system memory.

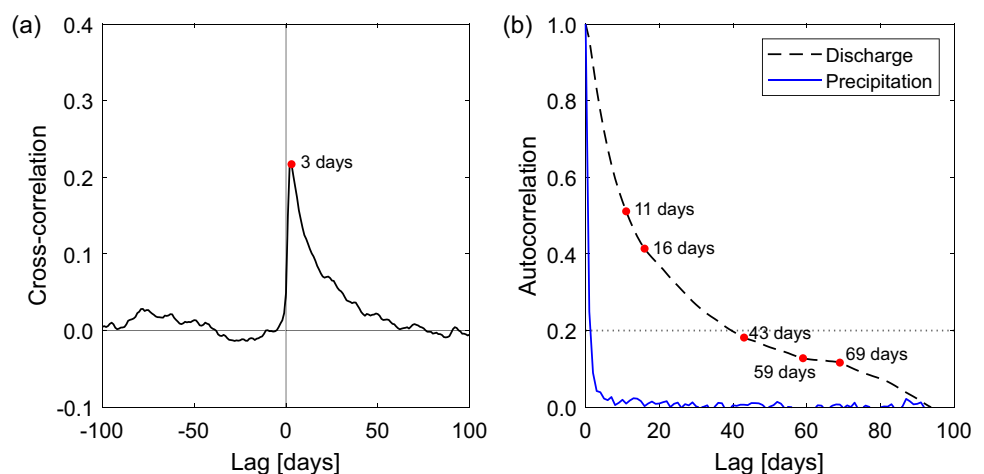
Discharge and climate trends

The annual mean air temperature and total PET at Blautopf show a significantly increasing trend between 1952 and 2021 with a slope of 0.03 and 0.95 °C mm year⁻¹ (Fig. 4a). The annual total precipitation is highly variable and does not show a significant trend of changes (Fig. 4b). On average, around two-thirds of the annual total precipitation goes into the atmosphere via evapotranspiration and one-third of it recharges the aquifer (Table 2). The spring discharge shows a high variability in different time scales (monthly, seasonal, and annual). The annual mean discharge also does not show a significant trend of changes, with the maximum nearly four times the minimum.

The monthly discharge and climate variables (Fig. 4c–e) show that June, July, and August are the warmest and also wettest months of the year. The mean discharge in these months is however lower than the annual mean rate (1.7 cf. 2.3 m³ s⁻¹). August to October have the lowest discharge (1.2 m³ s⁻¹ on average) of the year. March has the highest discharge but the lowest precipitation. It is also the month when the mean air temperature normally turns from negative to positive. Snowmelt thus plays a crucial role in generating the high discharge in March at the spring.

The daily mean air temperature at the catchment varies by nearly 50 °C between the minimum and maximum (from -23.0 to +26.7 °C; Fig. 4f). Nearly 20% of the days are below 0 °C and 40% of the days have no precipitation. The maximum daily precipitation is 81 mm and the highest 10% is more than 11 mm (Fig. 4g). The daily discharge

Fig. 3 Cross-correlation and autocorrelation functions of the daily precipitation and discharge from 1952 to 2021. **a** Cross-correlation function. **b** Autocorrelation functions of the precipitation and discharge and the red dots on it indicate the lags when the gradient of the function changes



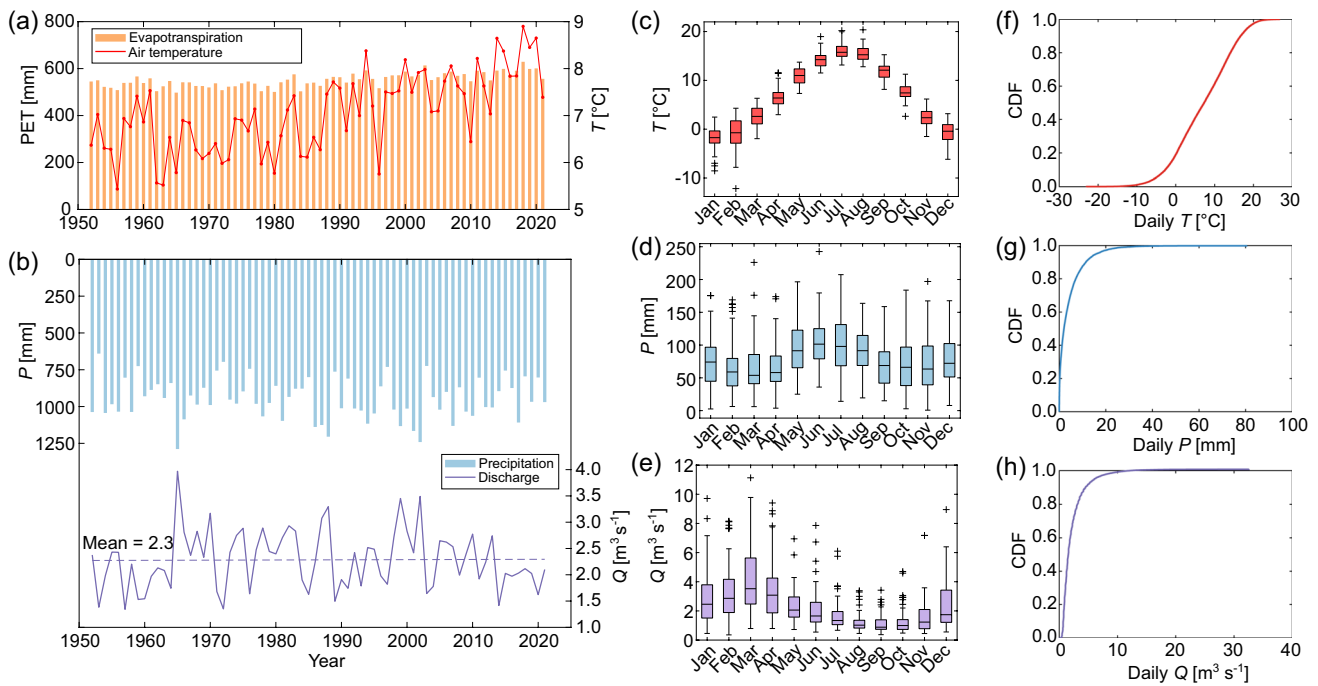


Fig. 4 The annual, monthly, and daily discharge and climates at Blautopf from 1952 to 2021. **a–b** The annual mean air temperature (T) and total potential evapotranspiration (PET); the annual total precipitation (P) and mean discharge (Q) with the average indicated (purple dashed

line). **c–e** The monthly mean air temperature, total precipitation, and mean discharge. **f–h** The cumulative distribution functions (CDFs) of the daily mean air temperature, total precipitation, and mean discharge

varies largely between 0.1 and $32.6 \text{ m}^3 \text{ s}^{-1}$, with an average of $2.3 \text{ m}^3 \text{ s}^{-1}$ (Fig. 4h). The 10th and 90th percentiles of the daily discharge are 0.7 and $4.7 \text{ m}^3 \text{ s}^{-1}$.

The annual, seasonal, and most of the monthly mean discharge and total precipitation show no significant trends of changes (Figs. S3–S5 in the ESM). The annual high (≥ 90 th percentile) and low discharge (≤ 10 th percentile) also show no significant annual trends of changes (Fig. S6 in the ESM). However, the discharge in January shows a significantly increasing trend, and that in April shows a significantly decreasing trend at the same rate of $0.02 \text{ m}^3 \text{ s}^{-1} \text{ year}^{-1}$ (Fig. 5). April is the last snow month of the catchment. The declining discharge in April is found because of the

significantly decreasing precipitation, increasing temperature and evapotranspiration.

The impact of snowmelt on discharge

Timing

The occurrence of peak spring discharge highly relates to the peak snowmelt at the catchment. The changing timing and intensity of the peak snowmelt under increasing temperature and decreasing snow can hence impact the peak discharge. The peak snowmelt normally occurs between December and April at Blautopf (Fig. 6a). Results show that nearly two-thirds ($n = 39$) of the daily discharge maxima were observed during and after the peak snowmelt within 1 week. The peak snowmelt period is counted from the day when the peak snow accumulation (measured in SWE) is observed until it is entirely melted (e.g. Fig. 6b). The start day of the peak snowmelt shows no significant trend of changes (Fig. 6c), but the end day significantly shifts from March towards February (Fig. 6d). The duration of the peak snowmelt shows a significantly declining trend at a rate of $-0.13 \text{ days year}^{-1}$ (Fig. 6e). The peak snowmelt lasts 17 days on average in the first 20 years (1950–1970) but only 13 days in the last 20 years (2000–2020), showing a long-term average of 15 days. Overall, the peak snowmelt is shown to end earlier

Table 2 Minimum, mean, and maximum of the annual total precipitation (P), annual total potential evapotranspiration (PET), the difference between the annual total P and PET , annual mean air temperature (T), and annual mean discharge (Q) from 1952 to 2021

Items	Minimum	Mean	Maximum
ΣP [mm]	640	950	1,288
ΣPET [mm]	497	552	629
$\Sigma (P-PET)$ [mm]	143	398	659
T [°C]	5.4	7.0	8.9
Q [$\text{m}^3 \text{ s}^{-1}$]	1.3	2.3	4.0

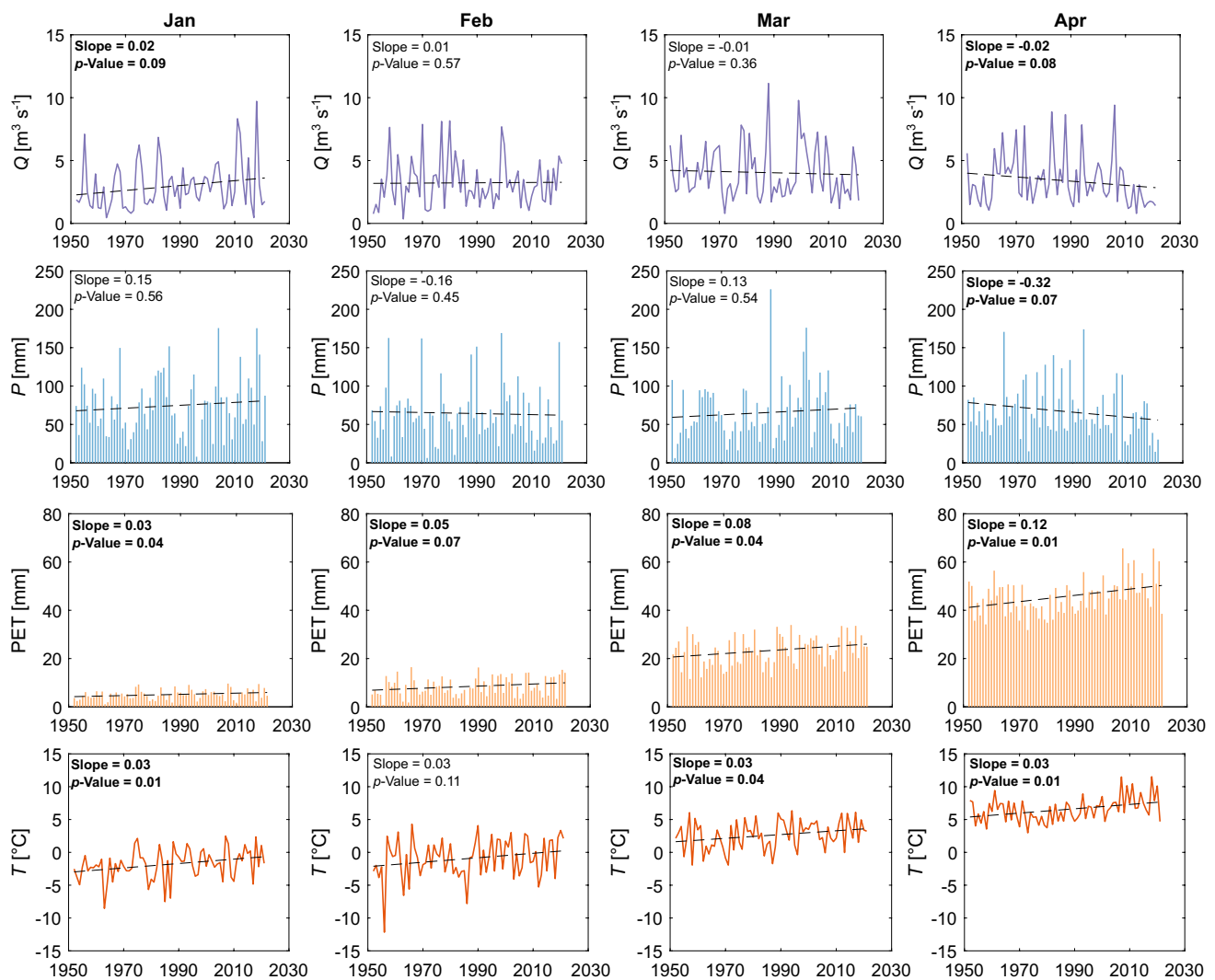


Fig. 5 Trends of the monthly mean discharge (Q), total precipitation (P), total potential evapotranspiration (PET), and mean air temperature (T) between January and April from 1952 to 2021. The dashed lines represent the trends

and last for a shorter duration. The peak discharge in the snow period is also found to onset earlier but this trend is not significant.

Intensity

The intensity of the peak snowmelt depends on the amount of the peak snow accumulation. Results show that around 3–23% of the annual total precipitation at Blautopf is snow, with a mean of 14% (Table 3). The peak snow accumulation is around half of the annual total snowfall on average. The highest peak snow accumulation at Blautopf was 181 mm recorded in 1988. This peak snow took only 14 days (close to the mean duration) to melt and generated the highest discharge rate ($32.6 \text{ m}^3 \text{ s}^{-1}$) at Blautopf on record. The peak snow accumulation shows a decreasing trend at all observed stations at a rate between -0.3 and $-0.8 \text{ mm year}^{-1}$ (Fig. S8

and Tables S3–S4 in the ESM). The most probable changing point was identified around 1988 and the peak snow accumulation has decreased by 35 mm on average since then (Fig. 7b). Around 85% of the peak snow accumulation was more than the daily precipitation maxima before 1988, but this rate has decreased to 75% after this year (Fig. S9 in the ESM). Despite that the daily precipitation maxima increasingly exceed the peak snow accumulation, they are mostly below the mean level (60 mm) of the latter. Overall, the peak snow accumulation at the catchment has shown a significant decreasing trend and the reducing magnitude has been especially severe since 1988.

The same changing point was identified in the annual snow-period (Oct–Apr) mean air temperature, which shows a significant increasing trend at a rate of $+0.03 \text{ }^{\circ}\text{C year}^{-1}$ (Fig. 7a). The coldest snow period ($-0.5 \text{ }^{\circ}\text{C}$) was observed in 1962 and the warmest snow period ($5.5 \text{ }^{\circ}\text{C}$) was in

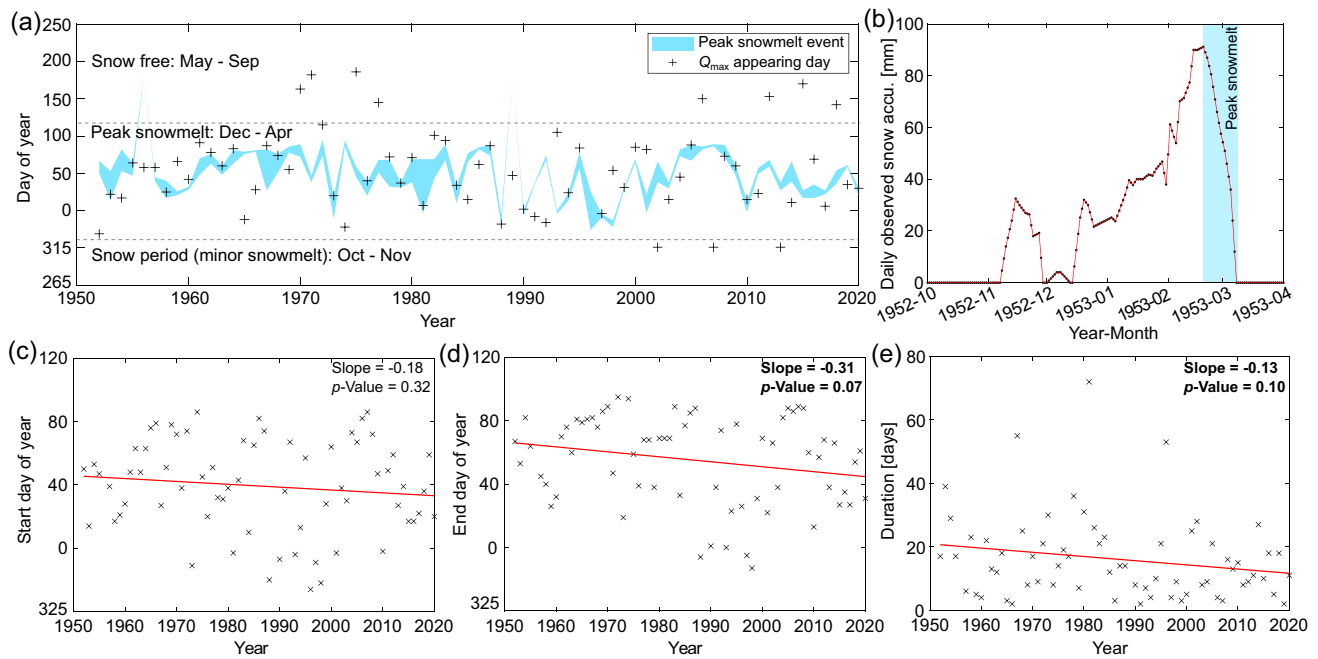


Fig. 6 Timing of the peak snowmelt and the daily discharge maxima (Q_{max}) from 1952 to 2020. **a** The peak snowmelt period and the appearance of the daily discharge maxima. **b** An example of the peak snowmelt in 1953 (blue block). The y-axis is the daily observed snow

accumulation (accu., measured in snow water equivalent). **c–e** The start day, the end day, and the duration of the peak snowmelt. The red solid line represents the trend. Note, a 1-year cycle is defined from July to June of the next year to cover a continuous snow period

2006. Starting from 1988, 70% of the annual snow-period mean air temperature was above the long-term median and increased by 1 °C on average. These results show that the catchment has entered a warm and low-snow state since then (Fig. 7a,b).

With the decreasing peak snow accumulation and increasing air temperature, the peak discharge in the snow period tends to decrease, but the trend is statistically not significant. Nevertheless, it has shifted towards the low state since 1988 (Fig. 7c). Around 80% of the peak discharge rates are lower than the long-term mean ($13.6 \text{ m}^3 \text{ s}^{-1}$) and have decreased by $1.1 \text{ m}^3 \text{ s}^{-1}$ on average since then. Before 1988, the peak snow accumulation was often above the long-term average

(60 mm) and melted slowly (~17 days) in a cold temperature (<2.3 °C); after this year, the peak snow accumulation was mostly below the average and melted faster (~13 days) in a warmer temperature (>2.3 °C). The multilinear regression between the peak snow accumulation, the snow-period mean air temperature, and the peak discharge (p -value < 0.01) shows that a 1-mm change in the peak snow accumulation results in $0.003 \text{ m}^3 \text{ s}^{-1}$ change in the peak discharge, and 1 °C change in the air temperature results in a $-1.8 \text{ m}^3 \text{ s}^{-1}$ change in the peak discharge. The low R^2 (0.2), however, indicates that the multilinear regression model explains little variance in the variables.

Karst discharge simulation in the past and future

The results of model calibration show that all 10,000 parameter sets give an $NSE \geq 0.70$ (Fig. S10 in the ESM). An optimum was found after exploring the whole parameter space, and the NSE of the optimum calibration is 0.74 and that of validation is 0.79 (Fig. 8). The NSE value indicates that 74% of the discharge changes at Blautopf have been explained by climate variations alone. The model has well captured the majority of the flow dynamics despite occasionally underestimating the extremely high discharges (Fig. 8 and Fig. S11 in the ESM). Overall, the model shows to be skillful in simulating the long-term discharge changes and the trend

Table 3 The annual peak snow accumulation (measured in snow water equivalent), total snowfall (measured in snow water equivalent), total precipitation, total number of days covered in snow, and the annual maximum discharge (Q_{max}) between 1952 and 2020. Note, a 1-year cycle is defined as spanning from July to June of the next year to cover a continuous snow period

Items	Minimum	Mean	Maximum
Peak snow accumulation [mm]	16	60	181
Total snowfall [mm]	19	132	295
Total precipitation [mm]	640	950	1,288
Number of days covered in snow	22	81	152
Q_{max} [$\text{m}^3 \text{ s}^{-1}$]	4.5	13.6	32.6

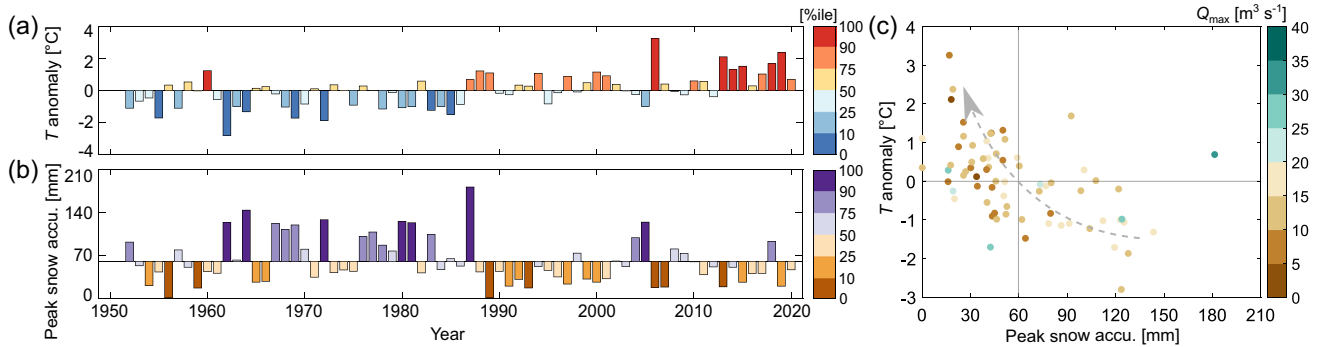


Fig. 7 The daily peak discharge (Q_{max}) of the snow period (Oct–Apr) have shifted to a low state due to increasing air temperature (T) and decreasing peak snow accumulation (accu., measured in snow water equivalent) between 1952 and 2020. **a** The annual snow-period mean air temperature anomaly relative to its long-term average (2.3 °C). **b**

The annual peak snow accumulation relative to its long-term average (60 mm). The interval of the legend is divided by the percentile (%ile) of the variables. **c** The relationship between the mean air temperature anomaly, the peak snow accumulation, and the daily peak discharge in the snow period

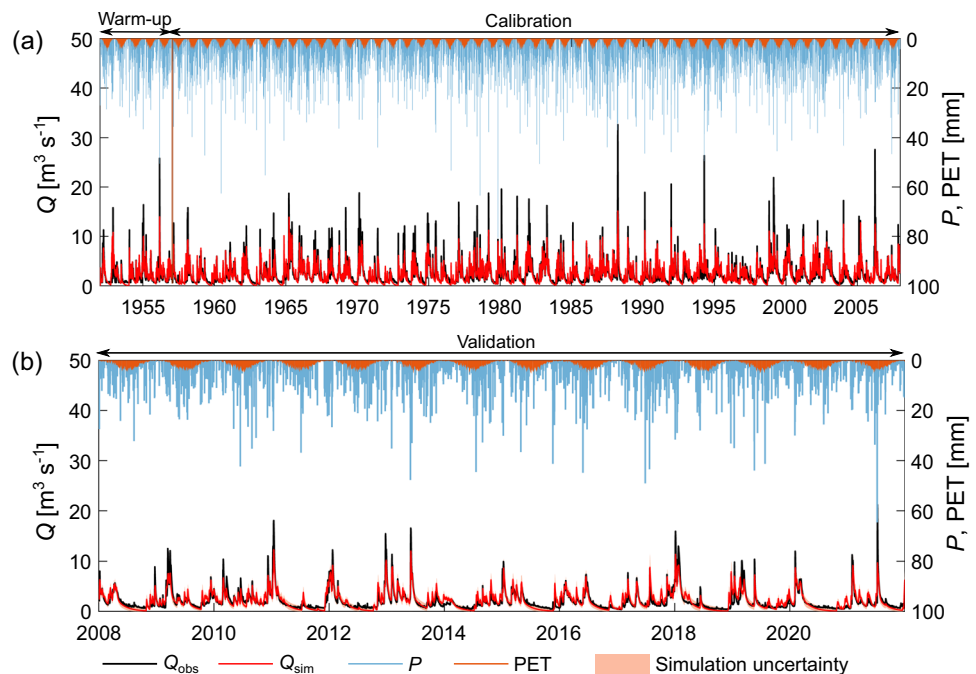
with only climate inputs, but caution is needed when using it to estimate the hydrologic high extremes.

The future projections simulated with the model show a substantially different warming degree between the climate change scenarios at Blautopf (Fig. 9): the annual mean air temperature is projected to increase by 0.5, 1.8, and 4.5 °C by the end of the twenty-first century for the RCPs 2.6, 4.5, and 8.5 respectively. The annual total precipitation is highly variable in the whole time series, showing no significant trend of changes for the RCPs 2.6 and 8.5, and a slightly increasing trend for the RCP 4.5 with a slope of 0.6 mm year⁻¹ (p -value: 0.04). The long-term average of the annual precipitation between 2000 and 2100 is shown

to be slightly higher (20–50 mm) than the observed annual mean (950 mm) between 1952 and 2021. The annual mean discharge also is shown to be highly variable under climate change, similar to the precipitation. In an extremely warming scenario of RCP 8.5, the annual mean discharge is projected to decrease at a rate of $-0.003 \text{ m}^3 \text{ s}^{-1} \text{ year}^{-1}$ (p -value: 0.06). The confidence interval shows the discrepancies between the projections of the adopted GCM-RCM members. The uncertainty due to climate models is ~10% for the projected annual mean air temperature, ~14–18% for the annual total precipitation, and ~35% for the annual mean discharge.

The annual minimum, mean, and maximum temperatures all increase with the climate change scenarios (Fig. 10a–c):

Fig. 8 The observed and simulated daily discharge under climate variations **a** in the warm-up (1952–1956) and calibration phases (1957–2007, NSE=0.74), and **b** in the validation phase (2008–2021, NSE=0.79) with simulation uncertainty, which is quantified as the differences between the maximum and minimum simulated discharges of all behavioural parameter sets ($n = 10,000$, NSE ≥ 0.70). Abbreviations: observed discharge (Q_{obs}), simulated discharge (Q_{sim}), precipitation (P), potential evapotranspiration (PET)



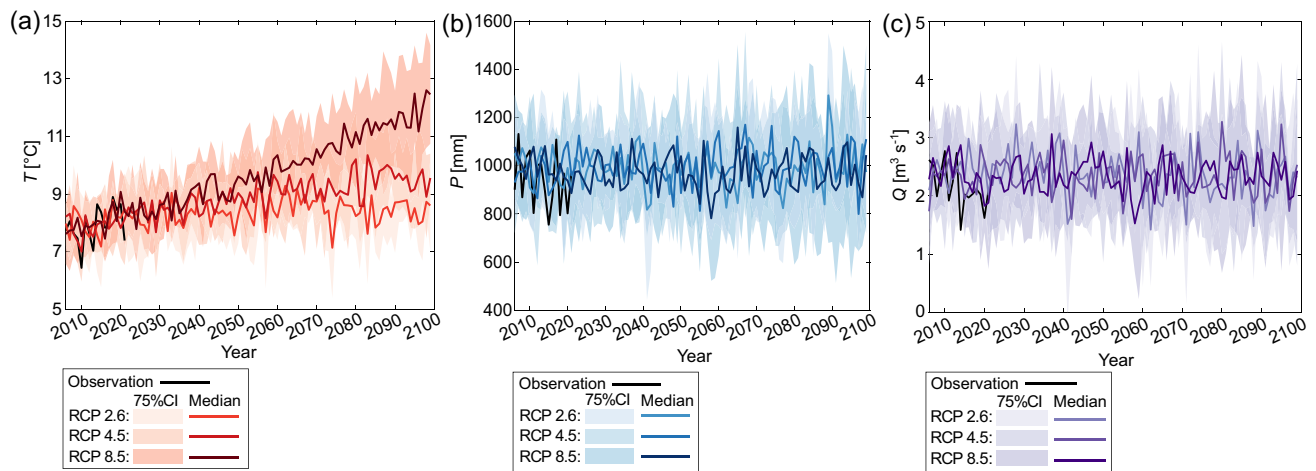


Fig. 9 The annual **a** mean air temperature (T), **b** total precipitation (P), and **c** mean discharge (Q) simulated under three climate change scenarios (RCPs 2.6, 4.5, and 8.5) between 2006 and 2100. The coloured lines represent the median of the simulation results of

all GCM-RCM members for each RCP; the coloured blocks represent the 75% confidence interval (CI) of all simulations; the black lines represent the observations

the annual minimum temperature is projected to increase between 0.3 and 3.4 °C, the annual mean temperature may increase between 0.4 and 3.1 °C, and the annual maximum temperature may increase between 0.3 and 3.7 °C for the three RCPs by the end of the twenty-first century. For the changes of precipitation by 2100 (Fig. 10d–f), the annual minimum precipitation (P_{\min}) slightly decreases with the intensifying climate change scenarios: P_{\min} (RCP2.6) > P_{\min} (RCP4.5) > P_{\min} (RCP8.5). The annual total precipitation (indicated by the median) is projected to decrease by around 2 and 4% (–22 mm and –36 mm) for RCPs 2.6 and 8.5, but to increase by 3% (+26 mm) for RCP 4.5. The annual maximum precipitation may increase by 4 and 5% (+0.7 and +0.9 mm) for RCPs 4.5 and 8.5, but shows no trend for RCP 2.6.

The annual minimum, mean, and maximum discharge all decrease with the intensifying climate change scenarios (Fig. 10g–i). The annual minimum discharge (indicated by the median) is projected to decrease by the end of the century by 43% (–0.21 m³ s^{–1}) for RCP 2.6, 35% (–0.17 m³ s^{–1}) for RCP 4.5, and 55% (–0.27 m³ s^{–1}) for RCP 8.5, compared with that (0.49 m³ s^{–1}) between 1952 and 2021. The annual mean discharge is projected to decrease by 4% (–0.10 m³ s^{–1}) to 10% (–0.22 m³ s^{–1}) for RCP 2.6 to RCP 8.5 by 2100. The annual maximum discharge is shown to change variably in each stage of the century, with a long-term average of ~6.7–7.0 m³ s^{–1} for the three RCPs. Compared with the long-term mean (13.6 m³ s^{–1}) between 1952 and 2021, the annual maximum discharge may decrease by ~50% projected by all three RCPs.

Discussion

Karst system structure

The Blautopf karst system responds quickly to precipitation in 3 days and also has a memory of 40 days. The quick response of discharge reveals that part of the karst system is highly karstified and forms fast flow paths, which are also supported by direct observations in the active conduit network and in-cave tracer tests (Lauber et al. 2014). Besides the fast flow, some rainfall infiltrates into the small fissures in the rocks and is released slowly to the spring (Larocque et al. 1998; Panagopoulos and Lambakis 2006). The rainfall signal is found to have significantly attenuated before the water discharges, as the newly recharged water has well mixed with the previous storage in the deep unsaturated zone (100–150 m), the large and deep phreatic conduits, and the underground lakes in the karst system. The hydrodynamic characteristics of the karst system summarised from correlation analysis (of discharge and precipitation) are also supported by the previous isotope study which traced the water flow from the surface to the discharge at this site (Schwarz et al. 2009).

Reliability of the groundwater model

In examining the adequacy of the groundwater model, the long-term observed daily discharge changes have been well simulated with only climate inputs in both calibration and validation phases (Fig. 8). The model proves to be

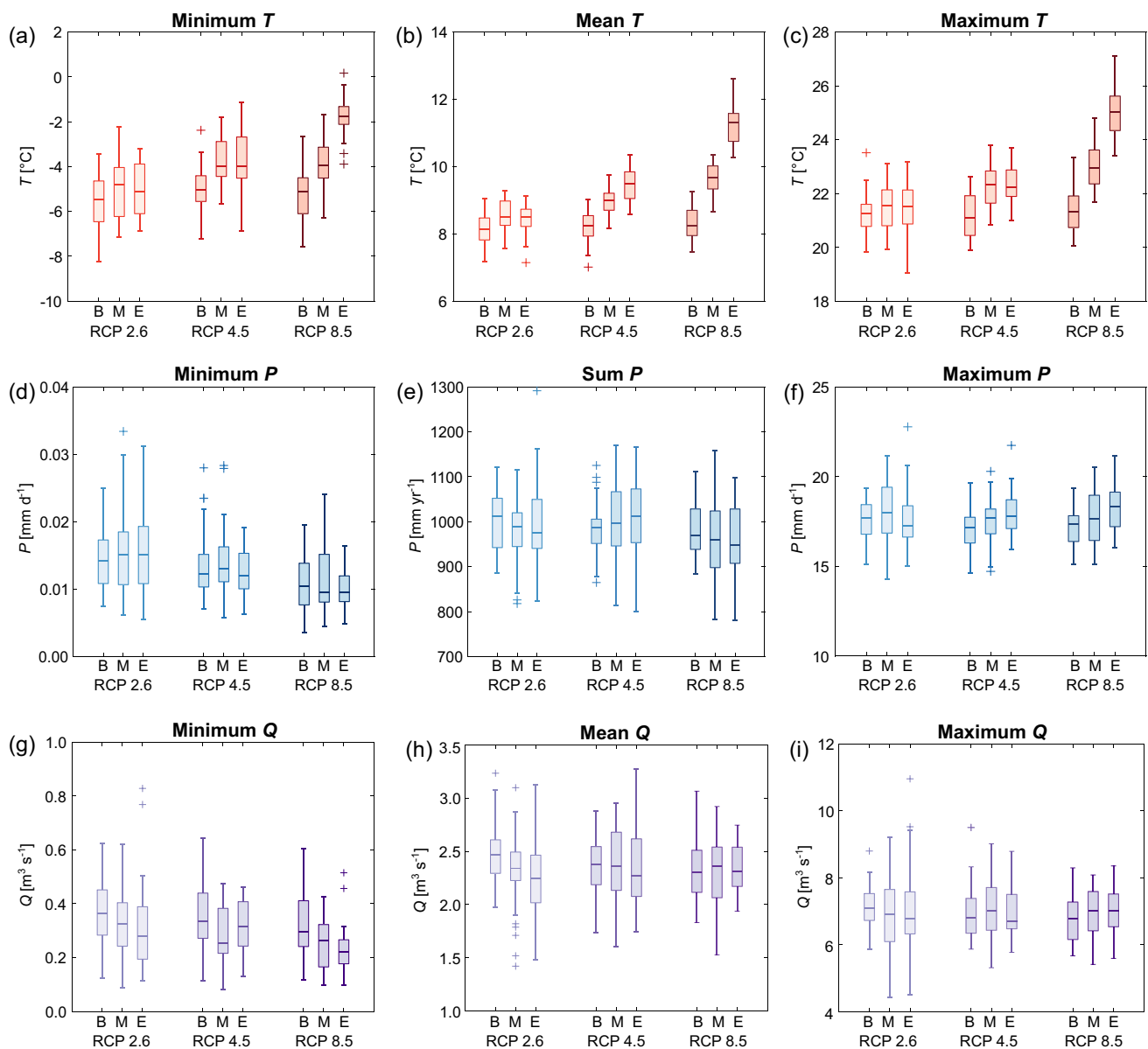


Fig. 10 The annual minimum (2.5th percentile), mean (or sum), and maximum (97.5th percentile) **a–c** air temperature (T), **d–f** precipitation (P), and **g–i** discharge (Q) at Blautopf simulated for three climate

change scenarios (RCPs 2.6, 4.5, 8.5) in the beginning (B, 2006–2039), middle (M, 2040–2069), and end (E, 2070–2100) stages of the twenty-first century

skillful in simulating the discharge in both low and mean flow but also occasionally underestimates the extremely high discharges (Fig. S11 in the ESM), which is a commonly known issue in hydrological modelling (Cinkus et al. 2023). Future simulations of such events may thus contain higher uncertainty. Additionally, the hydrodynamic characteristics of the karst system have been well simulated by the model, which is close to the historic analysis of the observed discharge and climate data (Figs. S12 and S13 in the ESM). Specifically, the modelled discharge reacts to the rainfall and snowmelt events the same as the observed discharge with a lag of 2–3 days; however, the

model has a system memory which is ~ 20 days longer than the observed site. This indicates that the model may need more time to return to the initial state after experiencing any disturbances; additionally, the calibrated model parameters (i.e. recession coefficients of the flows and recharge area) could potentially be useful for understanding the site and system properties. The calibrated catchment recharge area (164.70 km^2) is in good consistency with the results (165 km^2) from tracer tests and diving campaigns (Ufrecht et al. 2016), thus increasing confidence in the model.

The model however also shows a few caveats that may impact the future projections. For example, the model parameters show relatively high interactions with each other (Sobol sensitivity indexes in Table S6 in the ESM), theoretically indicating a lower identifiability of the parameters, which could be because of the simple and symmetric structure of the model (Fig. 2). The selection of this model structure is because (1) this structure is consistent with the previous literature (Schwarz et al. 2009) and expert knowledge of the system; (2) this structure gives the best model performance; (3) all calibrated parameters are sensitive and show an optimum (Fig. S10 in the ESM), and (4) the parameters that show relatively high interactions (i.e. k_{EM} , k_{MS}) could be potentially linked and interdependent by nature. For these reasons, this model structure is tentatively accepted but may contribute to uncertainty in future projections. Regarding the prediction uncertainty, some other factors can also play a role: (1) the parameters in the groundwater model and snow model are assumed as constant; however, changes in snow model parameters (e.g. DDF factor) may impact the partitioning of precipitation to snow and rainfall and thus influence the rate and timing of the peak discharge (Doumar et al. 2018); (2) the stationary assumptions of the system evolution (karstification) and the land use and land cover, which may change in the future and impact the hydrological processes; (3) and the model may struggle to simulate the extremely high and low flows because of lack of training for simulating such unobserved and challenging conditions.

Trends and mechanisms

The annual mean and minimum discharge of Blautopf do not show significant annual and seasonal trends of changes from 1952 to 2021, but rather they are projected to decrease by the end of the twenty-first century. In the scenarios of RCPs 2.6, 4.5 and 8.5, the annual mean discharge is projected to decrease by 4–10% and the annual minimum discharge may decrease by 35–55%. In contrast, the intensity of the annual high discharge has already been impacted by the warming climate and shifted to a low state ($<13.6 \text{ m}^3 \text{ s}^{-1}$) since the 1980s, and may decrease by 50% projected by all three scenarios in this century.

The changes of discharge at Blautopf could be attributed to its climatic and hydrogeologic settings. With the increasing temperature under climate change, the catchment evapotranspiration can be enhanced due to ~90% of the land surface being covered by forests and agriculture (Köberle 2005). As the annual total precipitation is projected to change slightly (–36 to +26 mm) at the catchment by the end of the century, the groundwater recharge may thus reduce due to increasing evapotranspiration (+60 to +147 mm) and the discharge may consequently decline. Besides that, the increasing temperature will not only

increase the evapotranspiration but also impact the timing and intensity of snowmelt. Despite that Blautopf is located at a relatively low altitude (600–800 m asl) and experiences less snow (~14% of the precipitation) compared with the alpine regions, the peak snowmelt still plays a crucial role in generating the annual peak discharge at the spring. In the past decades, the peak snowmelt has been shown to last for a shorter duration (–4 days) and has become less intense (–35 mm in peak snow accumulation). As a result, the peak discharge has shifted towards a low state. Despite that the daily precipitation maxima increasingly exceed the peak snow accumulation since 1988, they are mostly lower than the long-term average (60 mm) of the peak snow accumulation. With the increasing annual minimum temperature in winter (+0.3 to 3.4 °C by 2100), the peak discharge may continue decreasing by nearly half of the rate due to the less intense peak snowmelt under global warming.

This study has focused on quantifying the long-term response of the karst discharge to climate variations. To understand the detailed changes of the karst discharge in the dry and wet periods, future research may identify all likely changing points in the time-series discharge and climate data and analyse the step changes (Bonacci 2007). Additionally, our model is constrained to simulate the extremely high discharge. The future simulations of such events may hence contain higher uncertainty. Despite this caveat, the model still proves to be useful in estimating the system behaviour and the trends of discharge changes under climate change.

Implications

This study demonstrated the importance of quantifying the response of karst discharge to long-term climate change and variations. Catchments like Blautopf located in the temperate climate and mid-latitude may have been thought of as safe under climate change, compared with glaciers and arid zones (IPCC 2021). This study shows that despite the not significant historic trends of changes in the annual mean and minimum discharge, the annual peak discharge at the spring has reduced due to weakened peak snowmelt. If climate change continues, all types of discharge at the spring are projected to experience long-term adverse impact by 2100. The baseflow plays a crucial role in sustaining spring discharge, especially in the dry period. The decreasing minimum discharge may indicate water scarcity risks at the spring and pose threats to the groundwater-dependent ecosystems. The decreasing high discharge may warn of potential water supply risks for local communities and infrastructures, such as in southern Germany where karst aquifers and springs are taken as one of the main drinking water supplies (Fahrmeier et al. 2022).

Quantifying the local impact of climate change also allows for comparing the responses of karst discharge

at various climatic and geologic settings worldwide and understanding the variable impact of climate change. Due to limited lengths of karst discharge data and multiple influential factors (e.g. pumping), very few studies have quantified the long-term historic climate impact on karst discharge (Kimmeier and Bouzelboudjen 2001; Fiorillo et al. 2015, 2021). The karst spring discharge in central and southern Italy is found to have declined by 15–30% since 1987 (Fiorillo et al. 2015). Similarly, the Blautopf spring has experienced significant changes since 1988, but its annual mean discharge decreased by 4% ($-0.1 \text{ m}^3 \text{ s}^{-1}$) and the daily discharge maxima decreased by 8% ($-1.1 \text{ m}^3 \text{ s}^{-1}$). The annual mean discharge at the springs in Italy shows a significantly decreasing trend since the 1920s due to the drying climate (Leone et al. 2021), whereas this trend is not significant for Blautopf. These findings imply that southern Germany has experienced the adverse historic impact of climate change, although relatively slighter than the hotspots (e.g. Italy) in the Mediterranean.

When looking at the future projections in the twenty-first century, the annual low, mean, and high discharge at the karst springs in the Mediterranean are all projected to decrease, also the same for Blautopf, but their decreasing magnitudes are different. For example, the annual mean discharge is projected to decrease by 73% at a snow-governed semiarid site and by 36% at a site slightly impacted by snow in Lebanon (Doummar et al. 2018; Dubois et al. 2020), whereas at the karst springs in southern Greece and the West Bank in eastern Mediterranean, where they are almost not impacted by snow at all, the decrease may be 15–30% (Hartmann et al. 2012; Nerantzaki and Nikolaidis 2020). For Blautopf (southern Germany, temperate climate, snow-influenced), the annual mean discharge may decrease by 4–10% in this century. Despite the uncertainty, these findings suggest that the karst aquifers and springs in the Mediterranean are likely to experience severe depletion in the future climate scenario, while the sites more impacted by snow and located in more arid climates may experience larger reductions. These findings reinforce the need for maintaining and extending the groundwater monitoring networks for detection and management of groundwater changes under climate change.

Conclusions

In this study, a three-step integrated methodology has been established to quantify the long-term impact of climate variability and change on karst discharge from both historic and future perspectives, including (1) statistical analysis of the hydrodynamic characteristics of the karst system and the observed climates and discharge, (2) model calibration and evaluation with historic data analysis, and (3) simulations of

karst discharge under three climate change scenarios. This methodology has been applied to quantify the response of karst discharge at a snow-influenced temperate catchment (Blautopf) in central Europe from 1952 to 2100. The key findings of this study are:

- The Blautopf karst system, with a memory of 40 days, consists of both fast and slow flow paths that enable the discharge to respond quickly to precipitation in 3 days. The fast and slow flow components characterize the unique response of the karst aquifer to climate change and variations.
- The annual and seasonal mean discharge do not show a significant historic trend of changes. The monthly mean discharge shows that the discharge in April (the last month of the snow period) has significantly reduced ($-0.02 \text{ m}^3 \text{ s}^{-1} \text{ year}^{-1}$) due to decreasing precipitation and increasing air temperature and evapotranspiration. The annual mean discharge is projected to decrease by 4–10% (-0.10 to $-0.22 \text{ m}^3 \text{ s}^{-1}$) for the RCPs 2.6, 4.5 and 8.5 by 2100.
- The peak snowmelt plays a key role in generating the discharge maxima of the spring, but it is shown that it will end earlier (shift from March to February), last shorter (-4 days), and become less intense (-35 mm in peak snow accumulation). As a result, the annual peak discharge has shifted towards a low state ($<13.6 \text{ m}^3 \text{ s}^{-1}$) under global warming since 1988. The peak discharge may continue decreasing by 50% ($-7 \text{ m}^3 \text{ s}^{-1}$) as projected by all scenarios.
- The annual minimum discharge does not indicate a significant historic trend of changes; however, it is projected to decline by 35–55% (-0.17 to $-0.27 \text{ m}^3 \text{ s}^{-1}$) for RCPs 2.6, 4.5 and 8.5 due to increasing evapotranspiration.

Overall, this study shows the long-term historic and future impacts of climate change and variations for a snow-influenced temperate catchment in central Europe, and may suggest potential water scarcity risks at similar climatic and geologic settings (temperate climate, snow-influenced, large karst drainage area) worldwide. Despite that the impact is relatively milder compared with the Mediterranean region, quantifying and understanding the changes of karst aquifers and springs in this type of setting is necessary for mitigating the future impact of climate change.

Supplementary Information The online version contains supplementary material available at <https://doi.org/10.1007/s10040-023-02703-9>.

Acknowledgements The authors thank Mr. Guillaume Cinkus and Dr. Naomi Mazzilli for their helpful discussions and generous assistance with the *KarstMod* software and modelling, Dr. Andreas Wunsch for the GCM-RCM data acquisition, and Ms. Yanina Müller for providing details on the discharge measurements at Blautopf spring. The authors acknowledge the state environmental agency Landesanstalt für Umwelt

Baden-Württemberg (LUBW) in Germany for providing the karst discharge data.

Funding Open Access funding enabled and organized by Projekt DEAL. The authors acknowledge that the Melbourne Research Scholarship funded XF in the joint Ph.D. program between the University of Melbourne and Karlsruhe Institute of Technology (KIT), and thank the donors of the Justin Costelloe Award and the Diane Lemaire Scholarship granted to XF. The authors also acknowledge the support of the KIT-Publication Fund. Additionally, this paper is a contribution to the IMPART project of NG and NG who were funded by the German Research Foundation (DFG, project No. 432288610).

Declarations

Conflicts of interest On behalf of all authors, the corresponding author states that there is no conflict of interest.

Open Access This article is licensed under a Creative Commons Attribution 4.0 International License, which permits use, sharing, adaptation, distribution and reproduction in any medium or format, as long as you give appropriate credit to the original author(s) and the source, provide a link to the Creative Commons licence, and indicate if changes were made. The images or other third party material in this article are included in the article's Creative Commons licence, unless indicated otherwise in a credit line to the material. If material is not included in the article's Creative Commons licence and your intended use is not permitted by statutory regulation or exceeds the permitted use, you will need to obtain permission directly from the copyright holder. To view a copy of this licence, visit <http://creativecommons.org/licenses/by/4.0/>.

References

- Allen RG, Pereira LS, Raes D, Smith M (1998) Crop evapotranspiration: guidelines for computing crop water requirements. FAO Irrigation and Drainage Paper 56, FAO, Rome
- Amanambu AC, Obarein OA, Mossa J, Li L, Ayeni SS, Balogun O, Oyebamiji A, Ochege FU (2020) Groundwater system and climate change: present status and future considerations. *J Hydrol* 589:125163. <https://doi.org/10.1016/j.jhydrol.2020.125163>
- Armbruster V, Selg M, Bauer M, Schopper M, Straub R (2006) Untersuchungen zur Aquiferdynamik im Einzugsgebiet des Blautopfs (Oberjura, Süddeutschland) [Investigations on aquifer dynamics in the Blautopf catchment (Upper Jura, southern Germany)]. C98, Tübinger Geowissenschaftliche Arb (TGA), Tübingen, Germany
- Benavente J, Bosch AP, Mangin A (1985) Application of correlation and spectral procedures to the study of discharge in a karstic system (eastern Spain). *Karst Water Resour (Proc Ankara-Antalya Symp)* 161:67–75
- Bonacci O (2007) Analysis of long-term (1878–2004) mean annual discharges of the Karst Spring Fontaine de Vaucluse (France). *Acta Carsolog* 36:151–156. <https://doi.org/10.3986/ac.v36i1.217>
- Bonotto G, Peterson TJ, Fowler K, Western AW (2022) Identifying causal interactions between groundwater and streamflow using convergent cross-mapping. *Water Resour Res* 58:1–28. <https://doi.org/10.1029/2021WR030231>
- Brienen S, Walter A, Brendel C, Fleischer C, Ganske A, Haller M, Helms M, Höpp S, Jensen C, Jochumsen K, Möller J, Krähenmann S, Nilson E, Rauthe M, Razafimaharo C, Rudolph E, Rybka H, Schade N, Stanley K (2020) Klimawandelbedingte Änderungen in Atmosphäre und Hydrosphäre: Schlussbericht des Schwerpunktthemas Szenarienbildung (SP-101) im Themenfeld 1 des BMVI-Expertenetzwerks [Climate change-induced changes in the atmosphere and hydrosphere: final report of the key topic scenario development (SP-101) in the topic area 1 of the BMVI-Expert network]. <https://doi.org/10.5675/ExpNBS2020.2020.02>
- Çallı SS, Çallı KÖ, Tuğrul Yılmaz M, Çelik M (2022) Contribution of the satellite-data driven snow routine to a karst hydrological model. *J Hydrol* 607:127511. <https://doi.org/10.1016/j.jhydrol.2022.127511>
- Chen Z, Auler AS, Bakalowicz M, Drew D, Griger F, Hartmann J, Jiang G, Moosdorf N, Richts A, Stevanovic Z, Veni G, Goldscheider N (2017) The World Karst Aquifer Mapping project: concept, mapping procedure and map of Europe. *Hydrogeol J* 25:771–785. <https://doi.org/10.1007/s10040-016-1519-3>
- Chen Z, Hartmann A, Wagener T, Goldscheider N (2018) Dynamics of water fluxes and storages in an alpine karst catchment under current and potential future climate conditions. *Hydrol Earth Syst Sci* 22:3807–3823. <https://doi.org/10.5194/hess-22-3807-2018>
- Cinkus G, Wunsch A, Mazzilli N, Liesch T, Chen Z, Ravbar N, Doummar J, Fernández-Ortega J, Barberá JA, Andreo B, Goldscheider N, Jourde H (2023) Comparison of artificial neural networks and reservoir models for simulating karst spring discharge on five test sites in the Alpine and Mediterranean regions. *Hydrol Earth Syst Sci* 27:1961–1985. <https://doi.org/10.5194/hess-27-1961-2023>
- CollaudCoen M, Andrews E, Bigi A, Martucci G, Romanens G, Vogt FPA, Vuilleumier L (2020) Effects of the prewhitening method, the time granularity, and the time segmentation on the Mann-Kendall trend detection and the associated Sen's slope. *Atmos Meas Tech* 13:6945–6964. <https://doi.org/10.5194/amt-13-6945-2020>
- Collaud Coen M, Vogt FPA (2021) mannkendall/Matlab: Bug fix: prob_mk_n (v1.1.0). Zenodo. <https://doi.org/10.5281/zenodo.4495589>
- Deutscher Wetterdienst (2018) Kern-Ensemble v2018 [Core-ensemble v2018]. https://www.dwd.de/DE/klimaumwelt/klimaforschung/klimaprojektionen/fuer_deutschland/fuer_dtld_rcp-datensatz_node.html. Accessed Jan 2022
- Deutscher Wetterdienst (2021) Daily station data. <https://cdc.dwd.de/portal/>. Accessed Jan 2022
- Doummar J, Hassan Kassem A, Gurdak JJ (2018) Impact of historic and future climate on spring recharge and discharge based on an integrated numerical modelling approach: application on a snow-governed semi-arid karst catchment area. *J Hydrol* 565:636–649. <https://doi.org/10.1016/j.jhydrol.2018.08.062>
- Dubois E, Doummar J, Pistre S, Larocque M (2020) Calibration of a lumped karst system model and application to the Qachqouch karst spring (Lebanon) under climate change conditions. *Hydrol Earth Syst Sci* 24:4275–4290. <https://doi.org/10.5194/hess-24-4275-2020>
- Fahrmeier N, Frank S, Goeppert N, Goldscheider N (2022) Multi-scale characterization of a complex karst and alluvial aquifer system in southern Germany using a combination of different tracer methods. *Hydrogeol J* 30:1863–1875. <https://doi.org/10.1007/s10040-022-02514-4>
- Fiorillo F, Petitta M, Preziosi E, Rusi S, Esposito L, Tallini M (2015) Long-term trend and fluctuations of karst spring discharge in a Mediterranean area (central-southern Italy). *Environ Earth Sci* 74:153–172. <https://doi.org/10.1007/s12665-014-3946-6>
- Fiorillo F, Leone G, Pagnozzi M, Esposito L (2021) Long-term trends in karst spring discharge and relation to climate factors and changes. *Hydrogeol J* 29:347–377. <https://doi.org/10.1007/s10040-020-02265-0>
- Goderniaux P, Brouyère S, Wildemeersch S, Therrien R, Dassargues A (2015) Uncertainty of climate change impact on groundwater reserves: application to a chalk aquifer. *J Hydrol* 528:108–121. <https://doi.org/10.1016/j.jhydrol.2015.06.018>

- Goldscheider N, Chen Z, Auler AS, Bakalowicz M, Broda S, Drew D, Hartmann J, Jiang G, Moosdorf N, Stevanovic Z, Veni G (2020) Global distribution of carbonate rocks and karst water resources. *Hydrogeol J* 28:1661–1677. <https://doi.org/10.1007/s10040-020-02139-5>
- Green TR, Taniguchi M, Kooi H, Gurdak JJ, Allen DM, Hiscock KM, Treidel H, Aureli A (2011) Beneath the surface of global change: impacts of climate change on groundwater. *J Hydrol* 405:532–560. <https://doi.org/10.1016/j.jhydrol.2011.05.002>
- Hartmann A, Lange J, VivóAguado À, Mizyed N, Smiatek G, Kunstmann H (2012) A multi-model approach for improved simulations of future water availability at a large Eastern Mediterranean karst spring. *J Hydrol* 468–469:130–138. <https://doi.org/10.1016/j.jhydrol.2012.08.024>
- Hartmann A, Goldscheider N, Wagener T, Lange J, Weiler M (2014) Karst water resources in a changing world: review of hydrological modeling approaches. *Rev Geophys* 52:218–242. <https://doi.org/10.1002/2013RG000443>
- Hartmann A, Gleeson T, Wada Y, Wagener T (2017) Enhanced groundwater recharge rates and altered recharge sensitivity to climate variability through subsurface heterogeneity. *Proc Natl Acad Sci USA* 114:2842–2847. <https://doi.org/10.1073/pnas.1614941114>
- Hosseini SM, Ataie-Ashtiani B, Simmons CT (2017) Spring hydrograph simulation of karstic aquifers: impacts of variable recharge area, intermediate storage and memory effects. *J Hydrol* 552:225–240. <https://doi.org/10.1016/j.jhydrol.2017.06.018>
- IPCC (2014) Climate Change 2014: Synthesis Report. Contribution of Working Groups I, II and III to the Fifth Assessment Report of the Intergovernmental Panel on Climate Change]. IPCC, Geneva, Switzerland
- IPCC (2021) Summary for Policymakers. In: Climate Change 2021: the physical science basis. Contribution of Working Group I to the Sixth Assessment Report of the Intergovernmental Panel on Climate Change]. Cambridge University Press, New York
- Kendall MG (1955) Rank correlation methods. Charles Griffin, London, 196 pp
- Kimmeier F, Bouzelboudjen M (2001) A statistical time series analysis of hydro-climatic stress on karst aquifer system (Switzerland). 3rd Int Conf. Futurw Groundwater Resources Risk, Lisbon, Portugal
- Köberle G (2005) GIS-generierte Bodenkarte von Baden-Württemberg 1:25000 [GIS-generated terrain map of Baden-Württemberg 1:25000]. Blatt 7524 Blaubeuren. Karte mit Erläuterungen, Tübinger Geographische Studien 123, Universität Tübingen, Germany
- Kovačić G, Petrič M, Ravbar N (2020) Evaluation and quantification of the effects of climate and vegetation cover change on karst water sources: case studies of two springs in south-western Slovenia. *Water* 12:3087. <https://doi.org/10.3390/w12113087>
- Kumar CP (2012) Climate change and its impact on groundwater resources. *Int J Eng Sci* 1:43–60
- Larocque M, Mangin A, Razack M, Banton O (1998) Contribution of correlation and spectral analyses to the regional study of a large karst aquifer (Charente, France). *J Hydrol* 205:217–231. [https://doi.org/10.1016/S0022-1694\(97\)00155-8](https://doi.org/10.1016/S0022-1694(97)00155-8)
- Lauber U, Ufrecht W, Goldscheider N (2013) Neue Erkenntnisse zur Struktur der Karstentwässerung im aktiven Höhlensystem des Blautopfs [New insights into the structure of karst drainage in the active cave system of Blautopf]. *Grundwasser* 18:247–257. <https://doi.org/10.1007/s00767-013-0239-z>
- Lauber U, Ufrecht W, Goldscheider N (2014) Spatially resolved information on karst conduit flow from in-cave dye tracing. *Hydrol Earth Syst Sci* 18:435–445. <https://doi.org/10.5194/hess-18-435-2014>
- Leone G, Pagnozzi M, Catani V, Ventafridda G, Esposito L, Fiorillo F (2021) A hundred years of Caposele spring discharge measurements: trends and statistics for understanding water resource availability under climate change. *Stoch Environ Res Risk Assess* 35:345–370. <https://doi.org/10.1007/s00477-020-01908-8>
- Lorenzi V, Sbarbati C, Banzato F, Lacchini A, Pettita M (2022) Recharge assessment of the Gran Sasso aquifer (Central Italy): time-variable infiltration and influence of snow cover extension. *J Hydrol Reg Stud* 41:101090. <https://doi.org/10.1016/j.ejrh.2022.101090>
- Mahler BJ, Jiang Y, Pu J, Martin JB (2021) Editorial: advances in hydrology and the water environment in the karst critical zone under the impacts of climate change and anthropogenic activities. *J Hydrol* 595:125982. <https://doi.org/10.1016/j.jhydrol.2021.125982>
- Mangin A (1984) Pour une meilleure connaissance des systèmes hydrologiques à partir des analyses corrélatrice et spectrale [For a better understanding of hydrological systems using correlation and spectral analysis]. *J Hydrol* 67:25–43
- Mann HB (1945) Nonparametric tests against trend. *Econometrica* 13(3):245–259. <https://doi.org/10.2307/1907187>
- Martinez J (1960) The degree-day factor for snowmelt runoff forecasting. IUGG Gen Assem Helsinki, IAHS Publ. 51, IAHS, Wallingford, UK, pp 468–477
- Mazzilli N, Guinot V, Jourde H, Lecoq N, Labat D, Arfib B, Baudement C, Danquigny C, Dal Soglio L, Bertin D (2019) KarstMod: a modelling platform for rainfall–discharge analysis and modelling dedicated to karst systems. *Environ Model Softw* 122:103927. <https://doi.org/10.1016/j.envsoft.2017.03.015>
- Nash JE, Sutcliffe JV (1970) River flow forecasting through conceptual models, part I: a discussion of principles. *J Hydrol* 10:282–290. [https://doi.org/10.1016/0022-1694\(70\)90255-6](https://doi.org/10.1016/0022-1694(70)90255-6)
- Nerantzaki SD, Nikolaidis NP (2020) The response of three Mediterranean karst springs to drought and the impact of climate change. *J Hydrol* 591. <https://doi.org/10.1016/j.jhydrol.2020.125296>
- Olarinoye T, Gleeson T, Marx V, Seeger S, Adinehvand R, Allocca V, Andreo B, Apaéstegui J, Apoliti C, Arfib B, Auler A, Bailly-Comte V, Barberá JA, Batiot-Guilhe C, Bechtel T, Binet S, Bittner D, Blatnik M, Bolger T, Brunet P, Charlier JB, Chen Z, Chiogna G, Coxon G, De Vita P, Doummar J, Epting J, Fleury P, Fournier M, Goldscheider N, Gunn J, Guo F, Guyot JL, Howden N, Huggenberger P, Hunt B, Jeannin PY, Jiang G, Jones G, Jourde H, Karmann I, Koit O, Kordilla J, Labat D, Ladouche B, Liso IS, Liu Z, Maréchal JC, Massei N, Mazzilli N, Mudarra M, Parise M, Pu J, Ravbar N, Sanchez LH, Santo A, Sauter M, Seidel JL, Sivelle V, Skoglund RØ, Stevanovic Z, Wood C, Worthington S, Hartmann A (2020) Global karst springs hydrograph dataset for research and management of the world's fastest-flowing groundwater. *Sci Data* 7:59. <https://doi.org/10.1038/s41597-019-0346-5>
- Oudin L, Hervieu F, Michel C, Perrin C, Andréassian V, Anctil F, Loumagne C (2005) Which potential evapotranspiration input for a lumped rainfall-runoff model? Part 2, towards a simple and efficient potential evapotranspiration model for rainfall-runoff modelling. *J Hydrol* 303:290–306. <https://doi.org/10.1016/j.jhydrol.2004.08.026>
- Padilla A, Pulido-Bosch A (1995) Study of hydrographs of karstic aquifers by means of correlation and cross-spectral analysis. *J Hydrol* 168:73–89. [https://doi.org/10.1016/0022-1694\(94\)02648-U](https://doi.org/10.1016/0022-1694(94)02648-U)
- Panagopoulos G, Lambrakis N (2006) The contribution of time series analysis to the study of the hydrodynamic characteristics of the karst systems: application on two typical karst aquifers of Greece (Trifilia, Almyros Crete). *J Hydrol* 329:368–376. <https://doi.org/10.1016/j.jhydrol.2006.02.023>
- Peterson TJ, Western AW (2014) Nonlinear time-series modeling of unconfined groundwater head. *Water Resour Res* 50:8330–8355. <https://doi.org/10.1002/2013WR014800>
- Ravbar N, Kovačić G, Petrič M, Kogovšek J, Brun C, Koželj A (2018) Climatological trends and anticipated karst spring quantity and

- quality: case study of the Slovene Istria. *Geol Soc Lond Spec Publ* 466:295–305. <https://doi.org/10.1144/SP466.19>
- Saltelli A (2002) Making best use of model evaluations to compute sensitivity indices. *Comput Phys Commun* 145:280–297
- Schwarz K, Barth JAC, Postigo-Rebollo C, Grathwohl P (2009) Mixing and transport of water in a karst catchment: a case study from precipitation via seepage to the spring. *Hydrol Earth Syst Sci* 13:285–292. <https://doi.org/10.5194/hess-13-285-2009>
- Selg M, Schwarz K (2009) Am Puls der schönen Lau: zur Hydrogeologie des Blautopf-Einzugsgebietes [On the pulse of the beautiful Lau: on the hydrogeology of the Blautopf catchment]. *Laichinger Höhlenfreund* 44:45–72
- Sen PK (1968) Estimates of the regression coefficient based on Kendall's tau. *J Am Stat Assoc* 63:1379–1389
- Shapoori V, Peterson TJ, Western AW, Costelloe JF (2015) Decomposing groundwater head variations into meteorological and pumping components: a synthetic study. *Hydrogeol J* 23:1431–1448. <https://doi.org/10.1007/s10040-015-1269-7>
- Sobol IM (1976) Uniformly distributed sequences with an additional uniform property. *USSR Comput Math Math Phys* 16:236–242
- Stevanović Z (2019) Karst waters in potable water supply: a global scale overview. *Environ Earth Sci* 78:662. <https://doi.org/10.1007/s12665-019-8670-9>
- Taylor RG, Scanlon B, Döll P, Rodell M, van Beek R, Wada Y, Longuevergne L, Leblanc M, Famiglietti JS, Edmunds M, Konikow L, Green TR, Chen J, Taniguchi M, Bierkens MFP, MacDonald A, Fan Y, Maxwell RM, Yechieli Y, Gurdak JJ, Allen DM, Shamsudduha M, Hiscock K, Yeh PJF, Holman I, Treidel H (2013) Ground water and climate change. *Nat Clim Chang* 3:322–329. <https://doi.org/10.1038/nclimate1744>
- Toews MW, Allen DM (2009) Evaluating different GCMs for predicting spatial recharge in an irrigated arid region. *J Hydrol* 374:265–281. <https://doi.org/10.1016/j.jhydrol.2009.06.022>
- Ufrecht W, Bohnert J, Jan H (2016) Ein konzeptionelles Modell der Verkarstungsgeschichte für das Einzugsgebiet des Blautopfs (mittlere Schwäbische Alb) [A conceptual model of the karstification history for the Blautopf catchment (middle Swabian Alb)]. *Laichinger Höhlenfreund* 51:3–44
- Wunsch A, Liesch T, Broda S (2022) Deep learning shows declining groundwater levels in Germany until 2100 due to climate change. *Nat Commun* 13:1221. <https://doi.org/10.1038/s41467-022-28770-2>
- Xanke J, Liesch T (2022) Quantification and possible causes of declining groundwater resources in the Euro-Mediterranean region from 2003 to 2020. *Hydrogeol J* 30:379–400. <https://doi.org/10.1007/s10040-021-02448-3>
- Zhao K, Wulder MA, Hu T, Bright R, Wu Q, Qin H, Li Y, Toman E, Mallick B, Zhang X, Brown M (2019a) Detecting change-point, trend, and seasonality in satellite time series data to track abrupt changes and nonlinear dynamics: a Bayesian ensemble algorithm. *Remote Sens Environ* 232:111181. <https://doi.org/10.1016/j.rse.2019.04.034>
- Zhao K, Hu T, Li Y (2019b) Rbeast: Bayesian change-point detection and time series decomposition. <https://CRAN.R-project.org/package=Rbeast>. Accessed Jan 2022

Publisher's Note Springer Nature remains neutral with regard to jurisdictional claims in published maps and institutional affiliations.